Environmental Science and Ecotechnology 28 (2025) 100637

Contents lists available at ScienceDirect

Environmental Science and Ecotechnology

journal homepage: www.journals.elsevier.com/environmental-science-and-ecotechnology/

Original Research

Hydrogen excess drives metabolic reprogramming and viral dynamics in syngas-converting microbiomes

Gabriele Ghiotto *, Luca Francescato, Maria Agustina Biancalani, Laura Treu **, Stefano Campanaro

Department of Biology, University of Padua, Via U. Bassi 58/b, 35131, Padova, Italy

ARTICLE INFO

Article history:
Received 11 July 2025
Received in revised form
28 November 2025
Accepted 29 November 2025

Keywords:
syngas
metagenomics
metatranscriptomics
bacteriophage
defence systems

ABSTRACT

Microbial communities drive essential bioprocesses, including the conversion of synthesis gas into biomethane, a sustainable energy source that supports circular carbon economies. In anaerobic environments, specialized consortia of bacteria and archaea facilitate syngas methanation through syntrophic interactions, where hydrogenotrophic methanogens play a central role in reducing carbon dioxide and monoxide with hydrogen. However, imbalances in gas ratios, particularly excess hydrogen, can disrupt these interactions and impair overall efficiency. Yet, the molecular mechanisms underlying microbial responses to such imbalances remain poorly understood. Here we show that hydrogen excess triggers profound metabolic and viral remodeling in a thermophilic anaerobic microbiome, leading to reduced methane yields and ecological instability. This reprogramming involves transcriptional downregulation of methanogenesis genes in the dominant archaeon *Methanothermobacter thermautotrophicus*, coupled with upregulation of CRISPR-Cas and restriction-modification systems that correlate with diminished activity of an associated phage, indicating activated host defenses against viral threats. Concurrently, bacterial species such as those from Tepidanaerobacteraceae enhance carbon fixation via the Wood–Ljungdahl pathway, serving as electron sinks to mitigate redox imbalance. These adaptive responses highlight the microbiome's resilience mechanisms under stress, revealing viruses as both stressors and selective forces in syntrophic systems. Such insights advance our understanding of microbiome dynamics in bioconversion processes and guide the engineering of more stable microbial consortia for optimized syngas-to-methane conversion amid variable feedstocks.

1. Introduction

Synthesis gas (syngas) is a mixture primarily composed of carbon monoxide (CO), carbon dioxide (CO_2), and hydrogen (H_2). Through biomethanation, syngas is converted into methane (CH_4) [1]. This transformation is carried out under anaerobic conditions by specialized microbial consortia, particularly hydrogenotrophic and acetoclastic methanogens, which play a crucial role in the process [2,3]. Unlike thermochemical gas-to-methane conversion methods, biological biomethanation operates under milder temperatures and pressures, offering a more energy-efficient and environmentally friendly alternative. The process not only provides a sustainable route for renewable CH_4 production but also enables the valorization of syngas derived from biomass, waste, or industrial off-gases, contributing to the improvement of circular carbon economy strategies [4].

The composition of syngas depends on multiple parameters, including biomass feedstock, gasification conditions, and oxidizing agents, and may vary substantially during continuous operation [5]. For instance, high CO concentrations can be toxic to microorganisms in suspended cultures, posing a significant challenge to the stability of biomethanation [6]. Nevertheless, biological systems exhibit considerable flexibility, as both electron donors, H_2 and CO, can be fully converted to CH_4 regardless of their initial ratio. Optimal biomethanation is achieved when the syngas quality index (SQI) [7], defined as the molar ratio of electron donors to carbon donors in the syngas, is approximately 4. SQI values

* Corresponding author.
** Corresponding author.
E-mail addresses: gabriele.ghiotto@phd.unipd.it (G. Ghiotto), laura.treu@unipd.it (L. Treu).

https://doi.org/10.1016/j.ese.2025.100637

above 4 indicate an excess of reducing power, while values below 4 represent carbon-rich conditions. While recent research has probed the physiological limits of microbial syngas conversion under stress imposed by high CO or H_2 levels [8], the transcriptomic responses of the key microbial taxa to these compositional shifts remain largely unexplored.

Regarding microbial metabolism, CO catabolism can follow distinct biochemical routes [9,10]. In the acetate pathway, acetogenic bacteria such as *Clostridium*, *Acetobacterium*, and *Sporomusa* convert CO to acetate, which is subsequently consumed by acetoclastic methanogens. Alternatively, CO can be converted to H_2 and CO_2 via a biological water–gas shift reaction, also known as carboxydotrophic hydrogenogenesis, providing the substrate for hydrogenotrophic methanogens. Microorganisms such as *Rhodospirillum*, *Thermincola*, *Desulfotomaculum*, *Carboxydothermus*, *Carboxydocella*, and *Moorella* are known to carry out this route. Direct methanogenesis from CO as the sole carbon and energy source has been demonstrated only in three species to date: *Methanothermobacter thermoautotrophicus*, *Methanosarcina acetivorans*, and *Methanosarcina barkeri* [11,12]. Owing to its highly negative redox potential (E_0' of −524 to −558 mV for the CO_2/CO couple), CO is a potent energy source. The enzyme responsible for its reversible oxidation is the carbon monoxide dehydrogenase (CODH) [13–15], and the directionality of the reaction depends on cellular redox state and energy requirements. CODH contains a [Ni–4Fe–4S] catalytic cluster and is encoded by three main operons: *acs*, *cdh*, and *coo*. The *acs* and *cdh* operons code for subunits of the carbon monoxide dehydrogenase/acetyl CoA synthase (CODH/ACS) complex involved in the Wood–Ljungdahl (WL) pathway of carbon fixation [16,17], while the *coo* operon encodes a monofunctional CODH involved in energy metabolism via CO oxidation. Monofunctional CODHs oxidize CO to CO_2, transferring electrons to ferredoxins such as CooF. These are typically encoded together with *cooS*, which encodes the catalytic CODH subunit [18]. In contrast, the bifunctional CODH/ACS complex includes five subunits (AcsA/CdhA, AcsB/CdhC, AcsC/CdhE, AcsD/CdhD, and either AcsE or CdhB) and catalyzes both CO oxidation and carbon fixation by synthesizing acetyl-CoA from CO, a methyl group, and coenzyme A [19,20]. CdhB is typically found in archaeal CODH/ACS complexes, while AcsE is more common in bacterial systems and functions as a methyltransferase. Although these metabolic pathways have been extensively investigated in monocultures, their behavior in mixed microbial communities and how different species respond to changes in syngas composition remains poorly understood, particularly at the transcriptomic level.

In this study, we combined genome-centric metagenomics and metatranscriptomics to investigate the short-term response of the microbiome to changes in syngas composition. Following the establishment of stable biomethanation under an SQI of 2.7, two additional conditions were tested: a near-optimal SQI of 3.8 and a H_2-rich condition with an SQI of 5.6. The transcriptomic analysis of the dominant species was performed with a focus on key metabolic pathways involved in syngas bioconversion, emphasizing the molecular response to excessive reducing power, and proposing a mechanistic interpretation. In addition, the microbial community's response in terms of genetic heterogeneity to shifts in syngas composition and the presence of active bacteriophages was investigated, providing a comprehensive view of microbiome dynamics under both optimal and suboptimal feeding conditions. Collectively, these findings improve our understanding of the molecular mechanisms underlying syngas biomethanation and establish a basis for future research aimed at optimizing the process.

2. Materials and methods

2.1. Microbial inoculum

The microbial community used in this experiment was obtained from a laboratory-scale trickle-bed reactor running at thermophilic conditions and adapted to syngas at the Technical University of Denmark. The initial inoculum was adapted to grow on a synthetic basic anaerobic medium supplemented with phosphate buffer 0.05 mol L^{-1}, yeast extract, and Wolin's vitamin solution to obtain a medium with a final pH of approximately 7. The experiment was performed in a fed-batch setup, at 55 °C with continuous agitation at 130 rpm. Initially, batches were fed daily with 750 mL of artificial syngas having the following volumetric composition: 110 mL (15%) CO, 120 mL (16%) CO_2, and 520 mL (69%) H_2, corresponding to an SQI 2.7.

2.2. Experimental setup and design

Every syngas composition tested (SQI 2.7, 3.8, and 5.6) was analyzed in four biological replicates, resulting in a total of 12 batches. Each replicate was prepared in 1 L bottles with an initial working volume of 200 mL. Bottles were filled with 144 mL of the medium, and the liquid was flushed for 10 min to guarantee anaerobiosis. All bottles were sealed with rubber stoppers and aluminum crimps. Before inoculation, the bottles were preheated to 55 °C to prevent the culture from suffering a temperature shock. Each bottle was inoculated with 50 mL of the microbial inoculum with 2 mL of yeast extract, 2 mL of Wolin's vitamin solution, and 2 mL of $Na_2S{\cdot}7–9H_2O$ 25 g L^{-1}. To verify the reliability of the growth rate measurements, a control was established by inoculating an additional bottle with the same microbial inoculum that had been pretreated with 5 min of microwave exposure to ensure microbial inactivation (hereafter referred to as Blank). The fed-batch reactors were incubated at 55 °C in an orbital shaker (NBIOTEK NB-T205L, Korea) with constant agitation of 130 rpm. Initially, all the cultures were fed daily with a syngas mixture with SQI of 2.7 (A_pre). After twelve days, once the microbiome was displaying stable growth and CH_4 production, a shift in the feeding composition was performed by testing three different SQIs. The first condition was maintained with an SQI of 2.7 (A_post), while the second was adjusted to an SQI of 3.8 (B_post, 9% CO, 13% CO_2, 78% H_2) and the third to 5.6 (C_post, 5% CO, 11% CO_2, 84% H_2). To ensure precise feeding every day, the atmosphere of the batches was flushed with N_2 for 30 min to remove any residual gas in the headspace before feeding.

2.3. Analytical measures

The headspace pressure of the batches, as well as the gas composition, was measured daily, both before and after feeding, using a manometer (HD 2124.2, Delta Ohm, Italy). Ten milliliters of the headspace gas were collected from the bottles and analyzed using a gas chromatograph (Agilent Technologies 8860 GC, CA, USA) equipped with a thermal conductivity detector. The gas separation was performed using three micropacked columns, namely Hayesep Q (1.5 m, 1/16″ outer diameter [OD], −1.0 mm inner diameter [ID]), Hayesep N (0.5 m, 1/16″ OD, −1 mm ID), and MolSieve 5 Å (1.5 m, 1/16” OD, 1.0 mm ID), all using helium as carrier gas. For the volatile fatty acid analysis, 1 mL of the liquid sample was first acidified with 40 μL of orthophosphoric acid (85%, Sigma-Aldrich, MO, USA) and then centrifuged at 13,000 rpm for 10 min. Then, 1 mL of supernatant was transferred into a vial, and

100 μL of isocaproic acid (99% Sigma-Aldrich, MO, USA) was added as an internal standard. The concentrations were determined using a gas chromatograph (Agilent Technologies 8860 GC, CA, USA) equipped with a flame ionization detector and a DB-FFAP fused silica capillary column (30 m, 0.25 mm ID, 0.25 μm film thickness), with helium serving as the carrier gas. The growth rate of each fed-batch was measured in triplicate using 125 μL of the liquid phase per replica with a Tecan SPARK microplate reader at a wavelength of 600 nm. To maintain optimal conditions for the microbial community, the pH was measured daily using a pH meter (Basic 20, Crison, Spain) and adjusted as necessary to keep it within the range 7–8 by adding HCl or NaOH (Supplementary Table S1).

2.4. DNA/RNA sample collection, extraction, and sequencing

To co-extract DNA and RNA, liquid samples were collected from every replicate of the three conditions on Day 12 (before the shift) and Day 14 (after the shift). The extraction was performed with the RiboPure-Yeast Invitrogen kit (Thermo Fisher Scientific, Waltham, MA, USA). An aliquot of each replicate was saved for DNA sequencing, and the remaining aliquots were treated with the RNA Clean & Concentrator-5 kit, which included a DNase I treatment (Zymo Research, Irvine, CA, USA), to remove residual genomic DNA and selectively recover the RNA. For each extract, both before and after DNase treatment, Nanodrop 2000 (Thermo Fisher Scientific, Waltham, MA, USA) and Qubit fluorometers (Thermo Fisher Scientific, Waltham, MA, USA) were used to assess purity and concentration, respectively. Ribosomal RNA was removed using FastSelect –5S/16S/23S Kit (QIAGEN GmbH, Hilden, Germany). Library preparation was performed using the Nextera DNA Flex Library Prep Kit (Illumina Inc., San Diego, CA, USA) at the DiBio sequencing facility (Department of Biology, University of Padova, Italy). The samples were then sequenced using the Illumina NovaSeq platform (2 × 150, paired-end).

2.5. Metagenomics assembly and binning

Illumina reads were filtered using Trimmomatic v0.39 [21] to remove adapters and low-quality reads. High-quality reads were assembled with Spades v3.15.5 [22]. Bowtie2 v2.2.5 [23] and SAMtools v1.15 [24] were employed to map the reads to the metagenome and for format file conversion. Binning was performed with MetaBAT2 v2.2.15 [25], VAMB v5.0.4 [26], Maxbin2 v2.2.7 [27], and Semibin2 v2.1.0 [28]. Bin refinement was performed using DAS_Tool v1.7, and the quality of reconstructed bins was assessed using CheckM2 v1.0.1 [29]. The set of medium-to high-quality metagenome assembled genomes (MAGs) was obtained through the dereplication step using dRep v3.4.0 [30], in accordance with the MIMAG standards [31]. GTDB-tk v2.4.0 [32] with database r226 was employed for taxonomic assignment. Relative abundance (RA) profiles for the reconstructed MAGs were computed with coverM v0.7.0 [33]. Gene prediction was performed with Prodigal v2.6.3 [34], followed by functional annotation via EggNOG-mapper v2.1.12 [35]. The Kyoto Encyclopedia of Genes and Genomes (KEGG) [36] served as the reference database for the metabolic functional reconstruction of the identified MAGs.

2.6. Analysis of viral genomes

Viral contigs were identified using geNomad v1.11.0 [37] (parameters: '–enable-score-calibration –conservative', database version 1.9) and further processed with CheckV v1.0.1 [38] (database version 1.5) for determining the genome quality. Viral genome selection was based on a minimum length of 2 kb (for sequences with direct or inverted terminal repeats) or 4 kb (for the remaining sequences) for *de novo* assembled contigs, previously assembled using both Spades v3.15.5 [22] and Megahit v1.2.9 [39]. Viral genomes were clustered into viral operational taxonomic units (vOTUs) according to the MIUViG guidelines [40] (95% average nucleotide identity, 85% aligned fraction) using vclust v1.3.1 [41] (parameters: -algorithm leiden –metric ani –ani 0.95 –qcov 0.85 –out-repr). The contigs identified as proviral by either geNomad or CheckV were also clustered into vOTUs and represent the set of integrated proviruses. RA profiles for the reconstructed vOTUs were computed with coverM v0.7.0 [33], and coverage values were calculated from the reads per base output × 151 bp. The lifestyle of phage vOTUs was predicted using BACPHLIP [42]. Host (bacterial and archaeal) and virus interactions were determined using the iPHoP v1.4.1 [43] integrated pipeline (version, database version v1.4.1). The resulting interactions were visualized using plotly v2.29.1.

2.7. Genome-centric metatranscriptomics

RNA-seq reads were filtered with Trimmomatic v0.39 [21] and aligned to the assembled MAGs using Bowtie2 v2.4.4 [23]. Transcripts per million (TPM) profiles for the reconstructed MAGs and vOTUs were computed with coverM v0.7.0 [33]. The resulting SAM files were converted to BAM using SAMtools v1.15 [24]. The *HTSeq-count* script from the HTSeq v2.0.5 [44] python package was employed to count the reads mapping to each gene. For transcriptome data analysis, DESeq2 v1.4.2 [45] was employed. Each MAG was processed independently, excluding genes with a cumulative count across all samples of 5 or fewer. Differential expression analysis was conducted using the Wald test, with a $\log_2$ fold change ($\log_2$ FC) computed by comparing gene expression of A_pre against A_post, B_post, and C_post. Significance was determined using the Benjamini–Hochberg procedure to control the false discovery rate, with genes considered differentially expressed if they met both thresholds: $|\log_2 FC| \geq 1$ and adjusted p-value <0.05. The total number of differentially expressed genes (DEGs) for the species of interest was calculated at the KEGG module level to provide a broader functional overview (see details in Supplementary Fig. S1). We then performed a gene-level investigation, selecting genes involved in methanogenesis (hydrogenotrophic, acetoclastic, and carboxydotrophic) and carboxylic acid oxidation (butyrate, propionate, and acetate) based on information available in the scientific literature.

2.8. Statistical analysis

Statistical analyses on biochemical parameters were conducted using Welch's t-test, which accommodates unequal variances and small sample sizes ($n = 3$ per group by default). For temporal comparisons, measurements from Day 12 were compared to Day 14 for each experimental condition, using the reported means and standard deviations to calculate the t-statistic, degrees of freedom, and two-sided p-values. Additionally, independent comparisons were made between different conditions at Day 14 to assess condition-specific differences. All p-values are reported alongside the corresponding means for clarity in Supplementary Table S2.

3. Results

3.1. Temporal tracking of biochemical dynamics in CO_2 biomethanation

A time-course experiment was conducted to assess the short-term effects of varying syngas ratios on the structure, activity, and resilience of the microbiome (Fig. 1a). The experimental setup

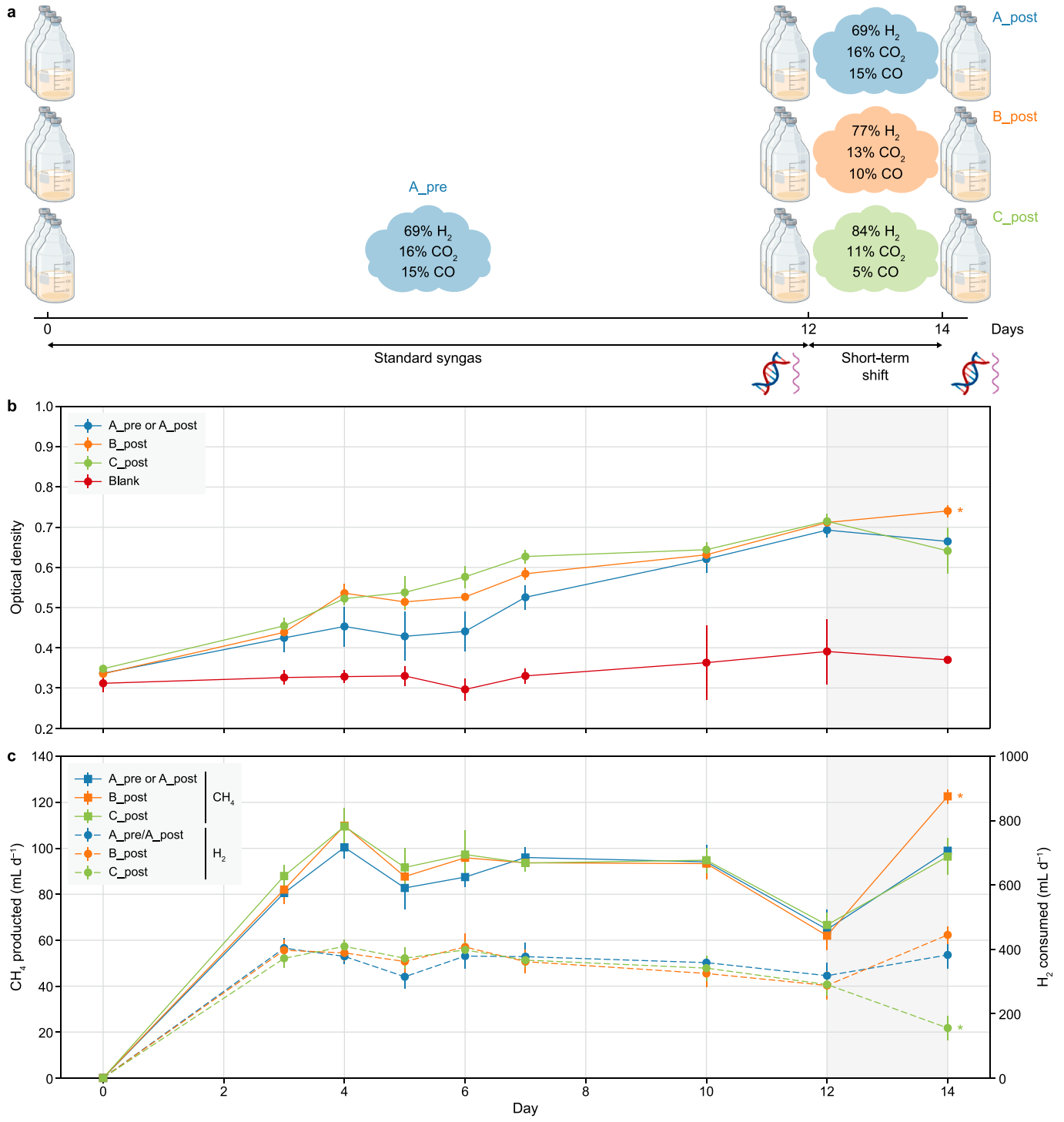

Fig. 1. Monitoring of microbial growth and biochemical parameters during operation at different syngas quality indices. a, Experimental design scheme. **b**, Average optical density. **c**, Average daily methane (CH_4) production and hydrogen (H_2) consumption expressed. The microbial communities investigated are highlighted by different colors: standard syngas composition (A_pre or A_post, blue), optimal H_2 concentration (B_post, orange), H_2 excess (C_post, green), and blank (red). Statistical comparisons were performed using Welch's *t*-test between Day 12 and Day 14, as well as independent comparisons between different conditions at Day 14. Statistically significant differences (*p*-value <0.05) are highlighted with an asterisk (*). The temporal period of the shift, from Day 12 to Day 14 was highlighted with a grey shadow. CO_2, carbon dioxide. CO, carbon monoxide.

included an initial adaptation phase (A_pre) during which a standard syngas composition (SQI = 2.7) was applied for 12 days. This was followed by a two-day exposure to three distinct conditions: a triplicate of near-optimal syngas ratios (SQI = 3.8, B_post), an H_2-excess condition (SQI = 5.6, C_post), and a control condition maintaining the original composition (SQI = 2.7, A_post). Process performance was systematically monitored, with particular focus on microbial growth rates, outlet gas composition, daily CH_4 production, and volatile fatty acid profiles (Fig. 1b and c). By tracking these key indicators, the microbial response to different syngas formulations was comprehensively characterized at the cellular level.

Consistent and sustained CH_4 production was observed throughout the adaptation phase (80–100 mg L^{-1} day^{-1}), with the highest conversion efficiency recorded under the B_post condition following the shift in syngas composition. Specifically, CH_4 production rates exceeded 120 mg L^{-1} day^{-1} in B_post, whereas both A_post and C_post conditions remained below 100 mg L^{-1} day^{-1} (Fig. 1c). A comparison between A_post and B_post CH_4, conducted via Welch's *t*-test for independent samples, yielded a statistically significant *p*-value ($p = 0.001$; Supplementary Table S2). In contrast, H_2 and CO_2 were almost completely consumed within 24 h, while CO was only partially consumed (Supplementary Table S1). No significant difference in CH_4 yield was detected between A_post and C_post, which is consistent with the observed decline in optical density on Day 14 in both microbiomes. When considering the input gases, CO consumption remained largely unaffected by excess H_2, whereas CO_2 consumption was reduced in C_post (Supplementary Table S1), suggesting that increased H_2 availability may constrain CO_2 reduction, consistent with thermodynamic or regulatory adjustments in hydrogenotrophic methanogenic metabolism. As far as growth, stable optical density was recorded for the B_post condition, when compared to the A_pre measure at Day 12, and the difference with A_post was statistically significant ($p = 0.005$, Supplementary Table S2). Instead, a modest decline was observed from A_pre to A_post, despite unchanged experimental conditions. This decrease likely reflects the natural decline of biomass over an extended period, including substrate depletion and maintenance energy demands, rather than treatment-specific effects. PCA revealed a distinct separation of samples according to time point and treatment condition, indicating substantial shifts in gas production and consumption throughout the experiment (Supplementary Fig. S2). Among the volatile fatty acids, acetic acid was the most predominant, showing a cumulative trend during the adaptation phase (~20 mg L^{-1}). Following the shift in syngas composition, both A_post and B_post conditions exhibited a reduction in acetic acid concentration (<15 mg L^{-1}), suggesting a change in its metabolism either due to a decrease in acetate production or an increase in its consumption (Supplementary Table S3). Butyric acid concentrations remained relatively stable throughout the experiment. Conversely, propionic acid peaked during the initial days (20–40 mg L^{-1}) and subsequently declined to levels below 5 mg L^{-1}. Isobutyric acid was consistently detected at minimal concentrations across all conditions.

3.2. Microbiome profiling during a change in gas feeding ratios

Genome-centric metagenomics was employed to investigate the microbiome composition during ongoing syngas biomethanation and to track its response to changes in the feeding ratios. The resulting assembly of the shotgun reads resulted in a total of 2.43 Gb, with an average alignment rate of 95%. The community was nearly entirely represented, a result mainly determined by its low complexity, which allowed for an exhaustive metabolic reconstruction. A low number of species was observed due to the combination of an adaptation period, the use of synthetic medium, and a simple carbon source for growth. A total of 68 MAGs belonging to 9 phyla were recovered (Supplementary Table S4), covering on average > 84% of the overall RA.

The community was dominated by *Methanothermobacter thermautotrophicus* SYN1, a hydrogenotrophic methanogen primarily responsible for the biomethanation process. Among the bacterial populations, the taxa with RA > 1% are Bacillota sp. SYN3, Desulfitobacteriales sp. SYN16, Haloplasmataceae sp. SYN21, *Coprothermobacter proteolyticus* SYN28, *Ureibacillus* sp. SYN30, and *Symbiobacterium* sp. SYN33. The most abundant members of the microbiome were also those with the highest transcriptional activity, with all these species exceeding 10,000 TPM in at least one time point (Supplementary Table S5). Among a few exceptions of low-abundant but highly active bacteria are members of the Tepidimicrobiaceae (spp. SYN5 and SYN18) and Tepidanaerobacteraceae (spp. SYN19 and SYN54) families, as well as Limnochordia sp. SYN41, Aneurinibacillaceae sp. SYN46, and Acetivibrionales sp. SYN63.

The activity of the microbiome was influenced by the varying ratios of supplied carbon sources (Fig. 2a). The most notable change was a reduction in the average transcript abundance of *M. thermautotrophicus* SYN1, which decreased from 551,178 to 285,040 TPM when comparing the A_pre and C_post conditions (Supplementary Table S5). In contrast, under C_post, species including *Ureibacillus* sp. SYN30, *Symbiobacterium* sp. SYN33, and Aneurinibacillaceae sp. SYN46 showed increased average transcript levels relative to other conditions. These observations suggest that when H_2 is present in excess, surpassing the optimal stoichiometric ratio (SQI = 4), the microbiome undergoes a transcriptional reorganization, likely reflecting a reduced reliance on hydrogenotrophic methanogenesis as the central metabolic pathway. Moreover, this excess of H_2 also affected the community composition. Species with increased transcriptional activity often displayed a corresponding rise in RA, whereas those with reduced expression either maintained stable abundances or declined. For instance, *M. thermautotrophicus* SYN1 decreased in RA from 77% to 67% between the A_pre and C_post conditions, while the RA of *Symbiobacterium* sp. SYN33 doubled, from 1.12% to 2.26% (Fig. 2b). The observation that some species display markedly higher or lower activity in B_post or C_post relative to A_pre should not be interpreted as evidence that all metabolic pathways within those microorganisms are proportionally up- or down-regulated. To validate the hypothesis of a metabolic shift and to elucidate the underlying mechanisms responsible for the observed patterns, a more in-depth transcriptomic analysis is required. It is essential to investigate the regulatory molecular processes and to determine how different syngas ratios influence CH_4 biogenesis.

3.3. Limited methanogenesis and stress-induced defense activation under elevated H2

Metatranscriptomics was conducted on the previously identified key microbial taxa to resolve their short-term response to incremental H_2 concentrations. The analyses focused on specific genes and pathways to provide a clearer understanding of the processes occurring within the different species (Fig. 3a and b). The changes in gene transcription level between post (Day 14) and pre (Day 12) conditions are represented as $\log_2$ FC calculated from three replicates, as well as those between the different post conditions (Materials and Methods section).

When considering *M. thermautotrophicus* SYN1, the number of DEGs identified in the comparison between A_pre and either A_post or B_post is negligible (lower than 30), highlighting that an increase in H_2 below the threshold does not negatively affect hydrogenotrophic methanogenesis. This is further confirmed by the increased CH_4 production in B_post on Day 14. Interestingly, the acetyl-CoA synthetase (*acs*) and the acetate transporter were both upregulated, with $\log_2$ FC values of +1.64 and + 2.46, respectively (Fig. 3c), suggesting that the hydrogenotrophic methanogen could consume the free acetate accumulated in the media to further boost its methanogenesis, as confirmed by the lower acetate concentration measured in B_post. Additionally, among the few upregulated genes, *hsdS*, which encodes the subunit S of a type I restriction enzyme, was particularly interesting

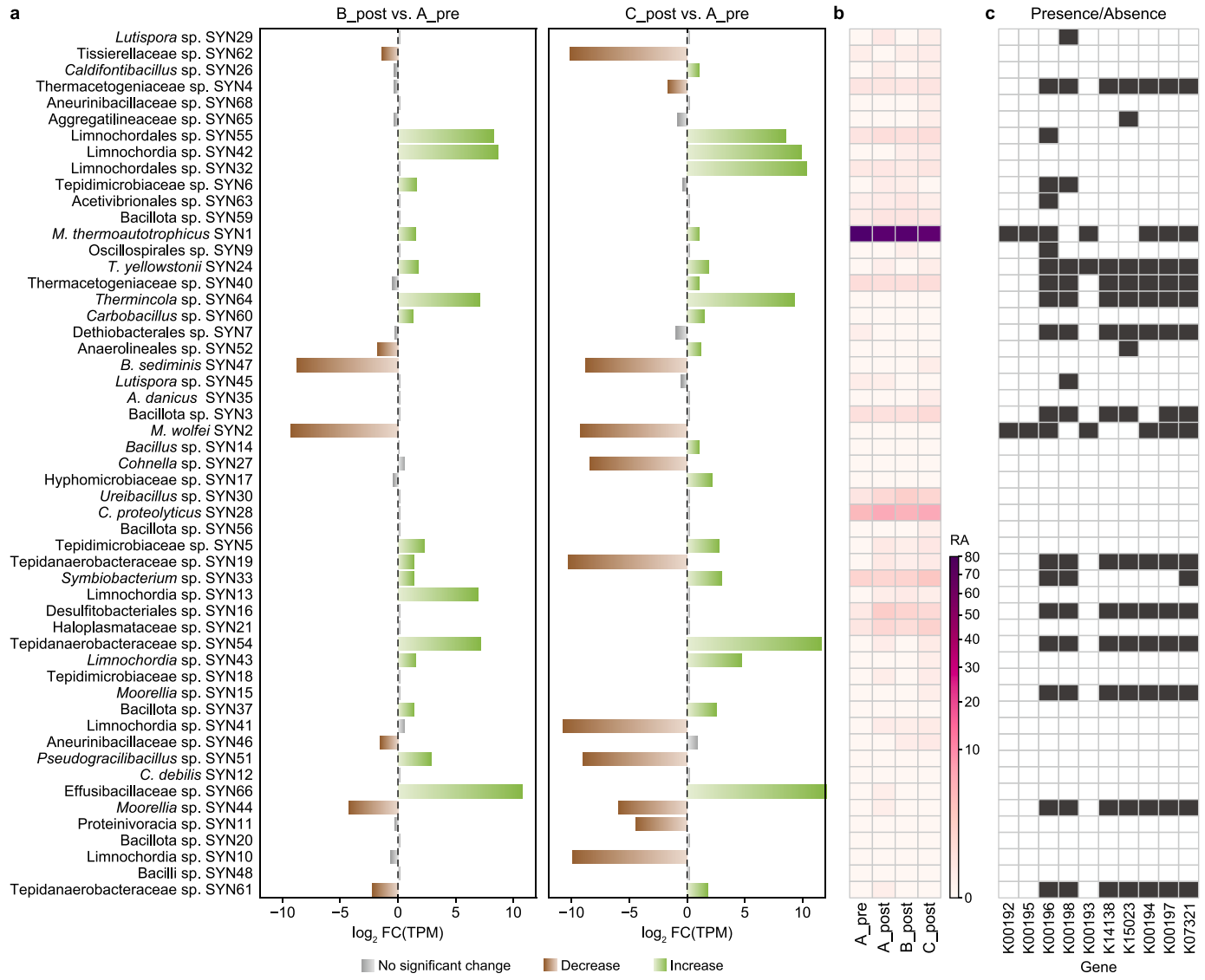

Fig. 2. Microbial dynamics during syngas biomethanation under varying gas feeding ratios. a, Log_2 fold change (log_2 FC) of the average expression level, as transcripts per million (TPM), between conditions A_pre and B_post or C_post. Three transcriptional response categories were identified: no significant change (grey, $-1 < log_2\ FC < 1$), increase (green, $log_2\ FC > 1$), and decrease (brown, $log_2\ FC < -1$) in activity. **b**, Average relative abundance (RA) of all metagenomes assembled genomes (MAGs) with RA $\geq$ 0.1 in at least one sample. **c**, Presence or absence of carbon monoxide-related genes in the MAGs. Black squares indicate gene presence. The correspondence between MAG and bin name is reported in Supplementary Table S4.

(log_2 FC = +3.05). This belongs to a larger group of deoxyribonucleases, involved in defense mechanisms against bacteriophages and other mobile elements. Conversely, a widespread downregulation of the hydrogenotrophic pathway was registered in C_post, both in the last step (*mcr*, *hdrA2B2C2*, *mvh*) as well as in the genes involved in the conversion from Formylmethanofuran to 5,10-Methylenetetrahydromethanopterin (*ftr*, *mch*, *mtd, frh*), all with log_2 FC < +1.00. (Fig. 3c). In C_post, *M. thermautotrophicus* SYN1 also evidenced an upregulation of multiple prokaryotic defense systems (Fig. 3d and e), including the CRISPR-Cas machinery (*cas1*, *cas2*, *cas3*, *csa3*, *cts2*, *cas6*), the type I restriction modification (RM) enzymes (*hsdS*, *hsdM, hsdR*), the cell division protein (*ftsZ*) and come endoribonucleases (i.e., *nob1*). This transcription pattern may be consistent with the presence of free foreign DNA, either of bacterial or viral origin, potentially reflecting biomass turnover or an active viral infection triggered by the stressful condition applied (i.e., excess of H_2). However, direct phage detection or identification of viral sequences from shotgun metagenomic data is essential to confirm the occurrence and ecological impact of such a hypothesis.

These findings align with defense-related gene profiles from other community members when comparing C_post against A_pre (Supplementary Table S6). For example, in Aneurinibacillaceae sp. SYN46, type I restriction-modification system genes (*hsdR*, *hsdM*) and a toxin-antitoxin module (*phd*) were upregulated. Tissierellaceae sp. SYN62 and *Ureibacillus* sp. SYN30 upregulated *ftsZ* and *mrr*, both of which are linked to stress response mechanisms. SYN63, a taxon showing substantial gene expression response to H_2 excess, harbored a CRISPR-associated protein gene (*csm4*), as well as numerous peptidase/inhibitor genes (*lspA*, *cwlO*, *asnB*, *IAL*, *blaR1*, *degP*, *dacC*, *hflC*), some of which may be upregulated under stress or during biomass turnover. Altogether, these defense and stress-related transcriptomic changes suggest a biological response to cellular damage or viral activation, potentially

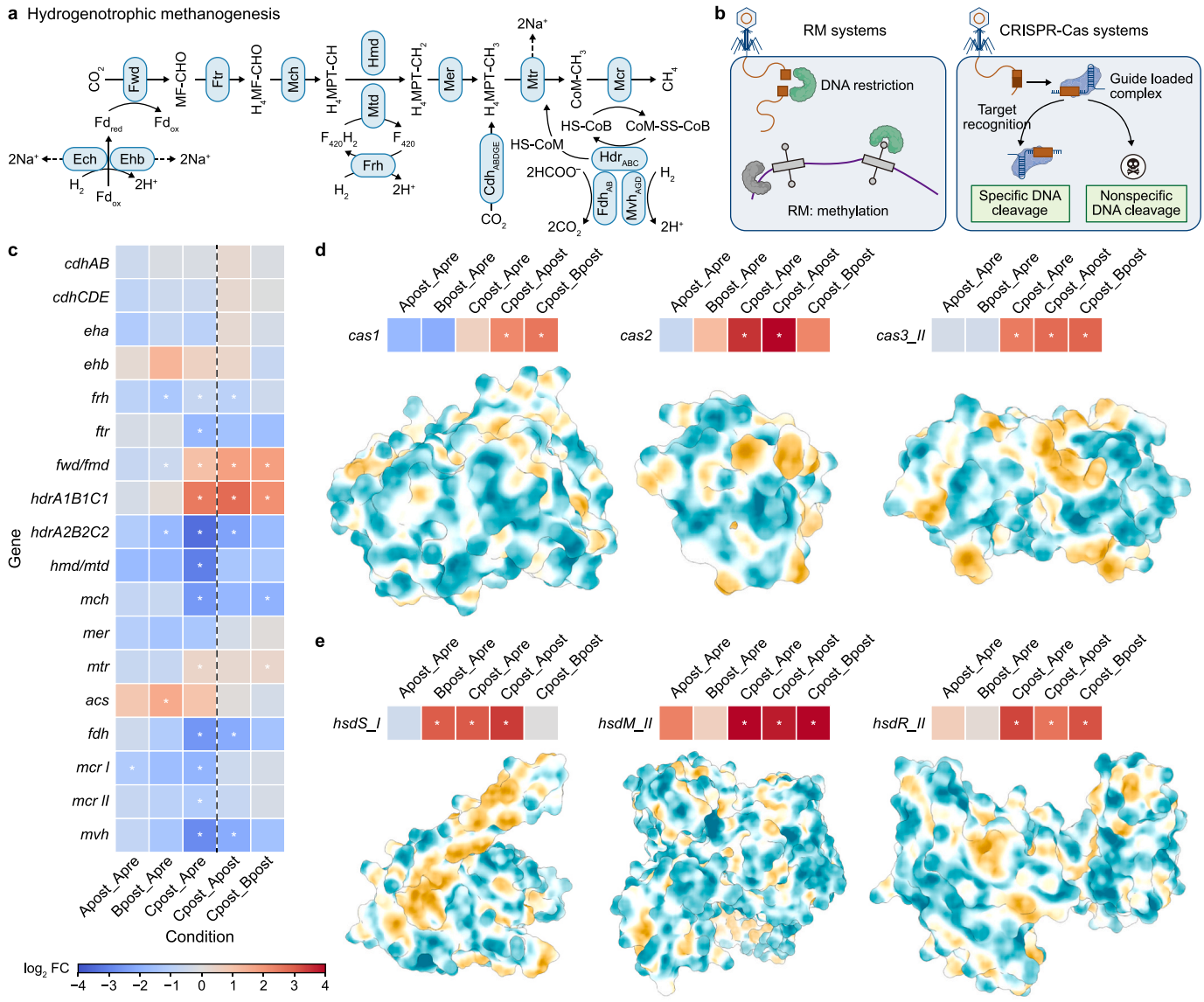

Fig. 3. Archaeal dynamics during syngas biomethanation under varying gas feeding ratios. a–b, Scheme of hydrogenotrophic methanogenesis (**a**) and archaeal defense systems (**b**) **c**, Changes in transcription of genes related to methanogenesis, carbon assimilation, and energy conservation, along with the results of the differential expression analysis, are presented as $\log_2$ fold change ($\log_2$ FC) values (Materials and Methods section). The $\log_2$ FC of multiprotein complexes is represented as the average value of all the detected subunits. Enzymes with statistically significant change in expression (p-value <0.05) are marked with an asterisk (*). **d–e**, The $\log_2$ FC is reported for genes upregulated in the C_post condition, including those encoding components of the CRISPR-Cas machinery (**d**) and restriction-modification (RM) enzymes (**e**). Differentially expressed genes (p-value <0.05) are marked with an asterisk (*). The enzyme surface is colored according to the hydrophobicity profile, and the structure was predicted with AlphaFold. CRISPR, clustered regularly interspaced short palindromic repeats. CO_2, carbon dioxide. CO, carbon monoxide. H_2, hydrogen. H_2O, water.

triggered by an excess of H_2 and the associated redox imbalance.

3.4. Coordinated upregulation of carbon fixation and CO metabolism pathways in acetogenic bacteria under H_2 excess

As previously observed, several bacterial species exhibited reduced activity under the H_2-excess condition C_post. Notably, *C. proteolyticus* SYN28 did not display significant alterations in its transcriptional profile. In contrast, Acetivibrionales sp. SYN63 demonstrated a substantial transcriptional response, with over 190 genes upregulated relative to the A_pre, A_post, and B_post conditions. Among these, the gene encoding the iron-sulfur subunit of the anaerobic carbon-monoxide dehydrogenase (*cooF*) was significantly upregulated ($\log_2$ FC = 5.160, p = 0.005), suggesting increased utilization of CO as a carbon and energy source. A similar transcriptional activation was observed in Tepidanaerobacteraceae sp. SYN19, which upregulated multiple genes associated with CO metabolism (Fig. 4a), including those encoding components of the CODH/ACS complex (*cdhD/acsD*), anaerobic carbon-monoxide dehydrogenase (*cooF*, *cooS*), CO-methylating acetyl-CoA synthase (*acsB*), 5-methyltetrahydrofolate Co-methyltransferase (*acsE*), and the CO dehydrogenase maturation factor (*cooC*). Likewise, in Tepidanaerobacteraceae sp. SYN54, the genes *cooF*, *cooS*, and *cooC* were upregulated in the C_post condition compared to both A_pre and B_post (Fig. 4a). In Tepidanaerobacteraceae sp. SYN61, *cooC*, and *cooS/acsA* were upregulated in C_post relative to A_pre, while CODH/ACS complex genes (*cdhD/acsD*, *cdhE/acsC*) were upregulated in C_post compared to B_post. The consistent upregulation of *coo* and CODH/ACS complex operons in the Tepidanaerobacteraceae taxon during the C_post condition likely represents a metabolic

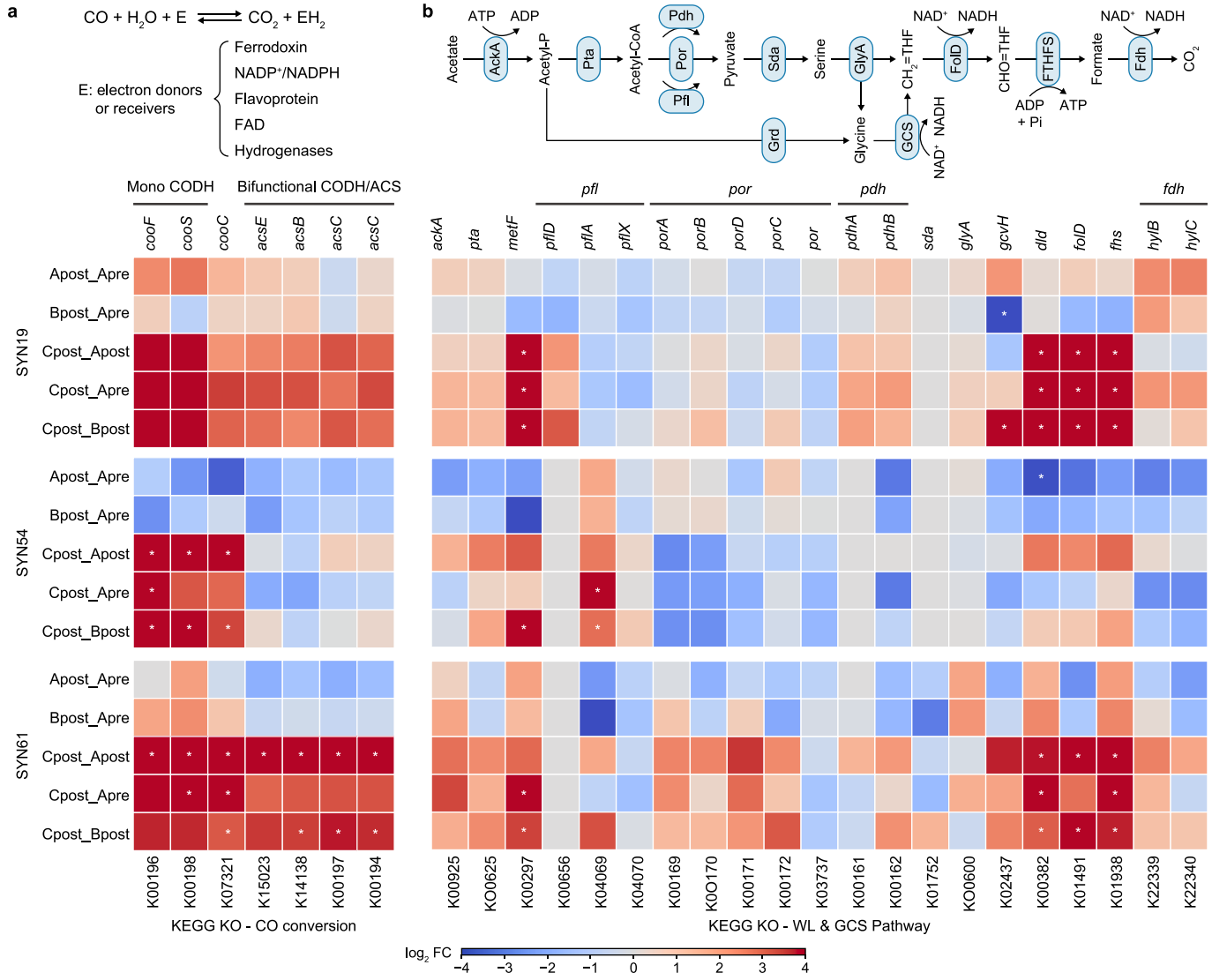

Fig. 4. Transcriptomic response of genes associated with the C-1 compounds fixation in prokaryotes. Changes in the transcription of genes related to methanogenesis, carbon assimilation, and energy conservation, along with the results of the differential expression analysis, are presented as log_2 fold change (log_2 FC) values (Materials and Methods section). The log_2 FC of enzymes composed of multiple subunits is represented as the average value of all the detected subunits. Enzymes with at least one differentially expressed gene with *p*-value <0.05 are marked with an asterisk (*). Values for mono- and bi-functional carbon monoxide dehydrogenase (CODH; **a**) and WL and WL/GCS genes (**b**) are reported for species belonging to the Tepidanaerobacteraceae taxon. FAD, Flavin adenine dinucleotide. WL, Wood–Ljungdahl. GCS, glycine cleavage system. CO_2, carbon dioxide. CO, carbon monoxide. H_2, hydrogen. H_2O, water.

adaptation to CO_2 limitation in the presence of excess electron donors (CO and H_2). Microorganisms capable of utilizing CO as an alternative carbon and energy source appear to activate these pathways to maintain carbon assimilation and energy conservation under reductive, CO_2-depleted conditions.

Another pathway central to the carbon metabolism experiencing a significant upregulation in the C_post condition in Tepidanaerobacteraceae species was the canonical WL, annotated as complete in these bacteria (Fig. 4b, Supplementary Fig. S3). Compared to B_post, SYN19 and SYN61 upregulated key WL genes, including methylenetetrahydrofolate reductase (*metF*), acetyl-CoA decarbonylase/synthase (*cdhD/acsD*, cdhE/acsC, *acsB*) and 5-methyltetrahydrofolate–corrinoid/iron–sulfur protein Co-methyltransferase (*acsE*), as well as the glycine cleavage system (GCS) associated dihydrolipoyl dehydrogenase (*dld*). Genes involved in formate assimilation, such as methylenetetrahydrofolate dehydrogenase (*folD*) and formate–tetrahydrofolate ligase (*fhs*), were also upregulated. Similarly, A_pre or A_post versus C_post comparisons revealed increased expression of WL genes (*metF*, *cdhD/acsD*, *cdhE/acsC*, *acsB*, *acsE*) and formate-related enzymes (*folD*, *fhs*). Notably, no significant upregulation was observed when comparing B_post to A_pre, indicating that only excess H_2, as in C_post, triggers this transcriptional response. These findings suggest that Tepidanaerobacteraceae species activate enhanced autotrophic carbon fixation via the canonical WL pathway, specifically under conditions of H_2 excess. The coordinated upregulation of enzymes in the carbonyl branch and formate metabolism genes evidences an increased reductive flux and energy conservation under H_2-rich conditions. Partial putative activity of the WL/GCS route has also been observed, although P- (*gcvP*, *gcvPA*, *gcvPB*) and T-protein (*gcvT*) genes, key components of the GCS, have not been annotated. This threshold-dependent response to H_2 availability has significant implications for syngas-fed bioreactors: increasing the H_2 supply beyond

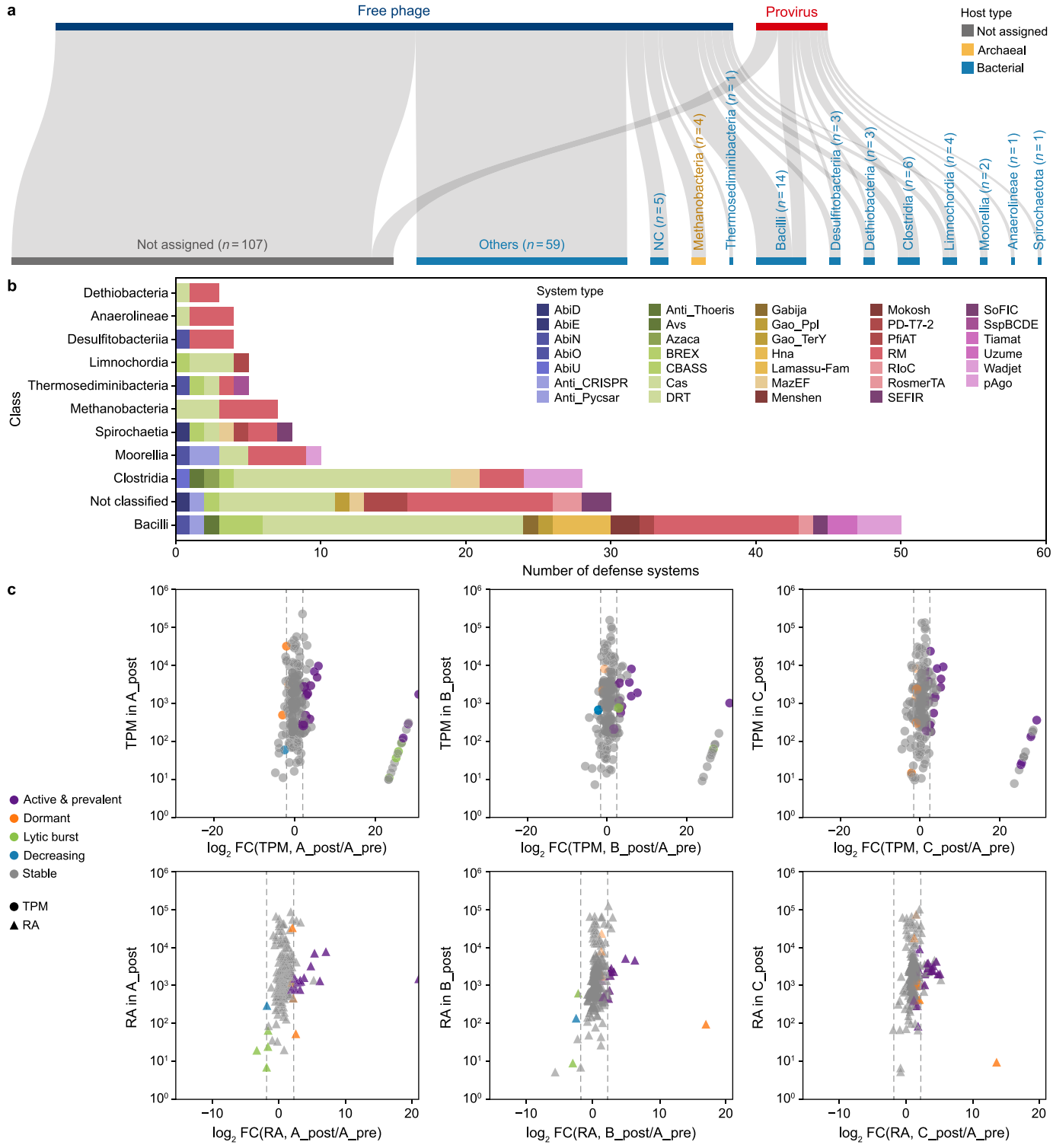

Fig. 5. Viral dynamics within the microbiome. a, Predicted virus–host associations, grouped at the Class level. Bacteriophages or prophages assigned to taxa not represented in the reconstructed metagenome assembled genomes (MAGs) were grouped in the category "Others". The number of viral entities associated with each taxonomic category is reported in brackets. **b**, Number of annotated prokaryotic defense systems in the MAGs associated with one or more phages or prophages. MAGs are grouped at the Class level to make visualization clearer. Each system is identified by a specific color. **c**, Activity and prevalence of the recovered viral genomes represented by transcript per million (TPM, circle) and relative abundance (RA, triangle), respectively. For each comparison of A_pre against either A_post, B_post, or C_post, the $\log_2$ fold change ($\log_2$ FC) of TPM or RA ratios has been computed and plotted against the value in the "_post" condition under examination. Four categories were highlighted: active and prevalent (purple), dormant (orange), lytic burst (green), decreasing (blue), and stable (grey).

stoichiometric requirements may stimulate key acetogenic populations, thereby enhancing carbon fixation efficiency and redirecting metabolic fluxes toward more reduced end-products. Understanding these regulatory thresholds can inform gas composition strategies to steer microbial community function and optimize syngas bioconversion processes.

3.5. Virome activity upon change in gas feeding ratios

Given the reported activity and upregulation of defense-related genes, we investigated the presence and potential role of phages in the microbial community. A total of 788 uncultivated viral genomes were recovered from assembled scaffolds and clustered into 190 vOTUs at species-level resolution. Of these, 20 vOTUs were identified as integrated proviruses, while the remaining 170 were predicted to be either virulent (72.6%) or temperate (27.4%) bacteriophages (Supplementary Table S7). Host-prediction analysis linked 83 Caudoviricetes vOTUs to bacterial and archaeal hosts spanning 12 classes (Fig. 5a). While we observed a maximum of 4 vOTUs per host, the mean overall vOTU per host ratio was 1 (median 0.614) reflecting the predominance of unique host associations for individual vOTUs. Taxonomic profiling of putative hosts showed broad phylogenetic diversity (Supplementary Table S8), including key taxa involved in anaerobic digestion, such as members of the Limnochordia, and two phages associated with *M. thermautotrophicus* SYN1.

A total of 36 distinct defense systems were identified and annotated across the 32 MAGs associated with at least one vOTU. The host classes Bacilli and Clostridia harbored the highest number of defense systems and exhibited the greatest number of associations with viral entities (Fig. 5b). Notably, comparative analysis of defense system types across taxonomic groups revealed that CRISPR (clustered regularly interspaced short palindromic repeats)-Cas systems and RM enzymes were the most prevalent, except for Desulfitobacteriia and Limnochordia, which lacked CRISPR-Cas and RM systems, respectively (Fig. 5b). Among the CRISPR-Cas systems identified and classified, type I-B was the most abundant (26%), followed by type III-D (12%). Additionally, the classes Methanobacteria, Symbiobacteria, and Anaerolineae exhibited a limited repertoire of defense mechanisms, primarily consisting of nucleic acid-targeting systems (i.e., Cas and RM). This contrasts with other species, which encoded a more diverse array of defense strategies, including phage protein sensing (AbiZ, Avs) and host integrity monitoring systems (e.g., toxins, retrons).

Comparison of A_pre with the "_post" conditions, based on trajectories of vOTU RA and activity, revealed distinct patterns of viral behaviour. (Fig. 5c–Supplementary Table S9–S10). Active & prevalent viruses were characterized by strong increases in both transcription and RA, with $\log_2$ fold changes in TPM ($\log_2$ FC(TPM)) and $\log_2$ fold changes in RA ($\log_2$ FC(RA)). Examples include phages predicted to infect Bacillota MAGs such as Desulfitobacteriales sp. SYN16 and Aneurinibacillaceae sp. SYN46. Notably, host abundances also increased relative to A_pre (Supplementary Fig. S4), suggesting that these taxa withstood viral pressure, likely through upregulation of RM defense systems (Supplementary Table S6). A second category, dormant viruses, was defined by increased DNA abundance but limited or absent transcriptional responses ($\log_2$ FC(RA) > 1.5 and $\log_2$ FC(TPM) < −1.5). These likely represent prophages or repressed infections, with virions accumulating without active expression. For instance, phages ms_7836 and mh_46334 increased in abundance in C_post (Supplementary Fig. S5), infecting Tepidimicrobiaceae sp. SYN18 and Limnochordales sp. SYN55, respectively. The stable RA of these MAGs across conditions supports the absence of productive infections. In contrast, the lytic burst group comprised vOTUs with strong transcriptional activation but declining DNA ($\log_2$ FC(TPM) > 1.5 and $\log_2$ FC(RA) < −1.5), consistent with rapid host lysis and subsequent DNA loss. The only representative was phage mh_5051 ($\log_2$ FC(TPM) = 1.8), predicted to infect *Pseudoclostridium thermosuccinogenes* SYN36. Host RA decreased in C_post, while viral RA and TPM remained stable in A_post, suggesting that infection was triggered after the environmental shift. The subsequent decline in both host and viral RA reflects population collapse following lysis (Supplementary Fig. S4–S5). A fourth category, declining viruses, showed simultaneous decreases in RA and transcription ($\log_2$ FC(TPM) < −1.5 and $\log_2$ FC(RA) < −1.5), likely reflecting loss of competitiveness or degradation of viral particles. Furthermore, two phages predicted to infect *M. thermautotrophicus* displayed intermediate behaviors outside these categories. Both showed raw transcription levels within the upper quartile of the TPM distribution (>815 TPM), averaging more than 13,000 TPM in C_post. The virulent phage mh_8355 showed moderate reductions in transcription ($\log_2$ FC(TPM) = −1.43) and abundance ($\log_2$ FC(RA) = −0.72), suggesting that replication was restricted by host defenses despite continued transcription. Conversely, the temperate phage mh_30781 maintained stable abundance ($\log_2$ FC(RA) = −0.10) but exhibited a discrete reduction in transcription ($\log_2$ FC(TPM) = −1.08), consistent with repression of lytic induction.

To rule out the potential effect of other mobile genetic elements on the upregulation of microbial defense systems, we investigated the presence and dynamics of plasmids. Of the 37 plasmid sequences recovered, 18 longer than 4000 bp were retained and clustered into 10 PTUs. Eight of these PTUs could be linked to putative hosts via predictions (Supplementary Table S11). When comparing plasmid abundance and transcription profiles (Supplementary Fig. S6) to those of their predicted hosts (Supplementary Fig. S4), two PTUs showed consistent increases across both metrics ($\log_2$ FC > 1.5). Specifically, plasmid ms_276 was associated with an unknown host, while plasmid mh_10344 was linked to *Aneurinibacillus danicus* SYN35 (Supplementary Table S11). Notably, *A. danicus* SYN35 also exhibited parallel increases in abundance and transcriptional activity in C_post (both $\log_2$ FC > 1.5), suggesting that this species thrives more efficiently under H_2-rich conditions. The co-increase of host and plasmid signals supports the idea that plasmid maintenance may provide selective benefits under these conditions, potentially by carrying accessory functions, such as stress resistance or metabolic traits, that reinforce host competitiveness. However, as no plasmids were linked to MAGs exhibiting upregulation of defense system genes, there is no evidence of a direct role of plasmids in driving prokaryotic defense responses in C_post.

Finally, when considering the metabolic potential of prokaryotic taxa infected by viruses, gene-level analysis reveals that phages target a notable fraction of species involved in carbon fixation pathways (Supplementary Table S8). Of these, nine WL-positive species (50%) and four WL/GCS-positive species (18%) are infected by phages. Conversely, among the 46 species that lack both WL and GCS pathways, 13 (28%) are infected by phages. Although phage infection is observed across both functionally relevant and non-relevant groups, the infection rate appears modestly higher in WL/GCS-positive species. This suggests a potential tendency of phages to target species with central metabolic roles. Given the ecological importance of these pathways, particularly in reductive metabolism where carbon and energy flows are tightly coupled, phage infections in these hosts could influence key ecosystem functions such as acetogenesis or syntrophic interactions.

4. Discussion and conclusion

Microbial consortia are central to bioconversion processes such

as syngas biomethanation; however, their functional stability can be compromised by environmental perturbations. Among these, variations in syngas composition remain underexplored, despite their potential to substantially alter microbial community structure and activity, which could lead to abrupt shifts or the extinction of key taxa involved in the methanation process. In this study, we provided an integrated analysis of microbial and viral dynamics within a thermophilic laboratory-scale bioreactor exposed to shifts in the $H_2/CO/CO_2$ feeding ratio, including both near-optimal and H_2-rich conditions. By combining metagenomics, metatranscriptomics, and virome analysis within a unified framework, we demonstrate how excess H_2 influences community reorganization at the level of key process-related genes and impairs ecosystem functionality.

Our results reveal that syngas composition, particularly H_2 concentration, exerts a profound influence on both microbial community structure and metabolic activity. Under standard and near-optimal $H_2/CO/CO_2$ ratios, 69/15/16 and 77/10/13, respectively, the bioreactors maintained a diverse and functionally robust consortium, characterized by the coexistence of hydrogenotrophic methanogens, acetogens, and syntrophic partners. This community configuration supports efficient carbon fixation and CH_4 production, as evidenced by the high transcriptional levels of key genes involved in methanogenesis (e.g., methyl-coenzyme M reductase) and carbon assimilation pathways (e.g., formate dehydrogenase and the CODH/ACS complex). This finding is consistent with thermodynamic and kinetic models of syngas methanation, which previously reported that CH_4 yield rises sharply as the H_2/CO_2 ratio approaches the stoichiometric value (SQI $\approx$ 4) but falls off when H_2 is in strong excess. Specifically, in trickle-bed reactors, increasing SQI from 1.44 to 3.67 has been shown to drive CH_4 content from 30% to over 70%, whereas a further increase above an SQI of 4 caused CH_4 to "plummet" back to 30% [7,46]. Likewise, we observed that an SQI of 3.8 yielded the highest volumetric CH_4 productivity and supported a stable microbiome, whereas at SQI of 5.6, unconverted H_2 accumulated (thermodynamic inhibition of CO conversion), and the community structure shifted. Under H_2-rich conditions, the methanogens reprogrammed their metabolism in response to stress, with *M. thermautotrophicus* downregulating its core methanogenesis, possibly reflecting feedback inhibition or an energetic shift when electrons are in extreme excess. Despite showing no variation in CH_4 production compared to the control condition (SQI = 2.7), the archaeon enters a state of thermodynamic imbalance, wherein excess H_2 can over-reduce electron carriers, leading to redox stress. This phenomenon has been previously demonstrated in the hydrogenotrophic archaeon *Methanocaldococcus jannaschii* [47]. Concomitantly, *M. thermautotrophicus* strongly upregulated stress and defense systems (CRISPR-Cas and RM genes). This suggests a heightened viral or phage pressure in the H_2-surplus regime. Stress conditions are known to induce prophage lytic cycles in anaerobic communities [48], with CRISPR-Cas and RM machinery providing adaptive immunity by recognizing invading nucleic acids [49]. Thus, high H_2 may have perturbed the archaeon (and the associated phages), triggering an antiviral response. This hypothesis is supported by the presence of a phage putatively linked to *M. thermautotrophicus*, which displays a decrease in both activity and abundance due to an effective counterattack by the host. Conversely, a fraction of the bacterial population responded to H_2 excess by ramping up carbon-fixation pathways. Notably, taxa such as Tepidanaerobacteraceae and Acetivibrionales increased expression of the canonical WL pathway genes, especially the carbonyl-branch (*acsB*, *acsC*, *acsD*, *metF*), as well as anaerobic carbon-monoxide dehydrogenases (*cooF*, *cooS*). This suggests that these bacteria were scavenging CO_2 (and possibly CO) to form acetyl-CoA/acetate, effectively serving as electron sinks under H_2 surplus. Such metabolic shifts are well aligned with known syntrophic behavior; in fact, many homoacetogens and syntrophic acetate oxidizers possess the WL pathway and can consume H_2 and CO_2 to produce acetate [50]. This scenario likely reflects a compensatory mechanism that buffers H_2 levels by fixing carbon and generating acetate, which cannot be uptaken by acetoclastic archaea, as they are absent in the community, and thus is exploited by the bacterial population for growth. The transcriptomic landscape emerging clearly shows that the risk of inhibition and process failure is not related to CO toxicity but to thermodynamic inhibition by excess H_2, as previously hypothesized but never verified with activity evidence [5,8].

Our findings build upon and refine the emerging picture from prior syngas biomethanation research. We confirm and expand on the hypothesis that high H_2 exerts a thermodynamic bottleneck by showing that significant methanogenic repression occurs. Concurrently, our data indicate possible lytic activity of multiple bacteriophages, suggesting that microbial communities are experiencing stress under these conditions, although further validation is required. This dual response supports a model of stress-induced collapse, in which excess electron donors destabilize both energetic and ecological balances. Our work thus bridges a critical gap between theoretical expectations and empirical observations, integrating virus-host dynamics with functional readouts of metabolism. Moreover, the knowledge gained holds potential applications in the biotechnological process under investigation, particularly in the context of phage therapy.

CRediT authorship contribution statement

Gabriele Ghiotto: Writing - Review & Editing, Writing - Original Draft, Visualization, Software, Methodology, Investigation, Formal Analysis, Data Curation, Conceptualization. **Luca Francescato:** Methodology, Investigation. **Maria Agustina Biancalani:** Methodology, Data Curation. **Laura Treu:** Supervision, Resources, Project Administration, Funding Acquisition, Conceptualization. **Stefano Campanaro:** Writing - Review & Editing, Writing - Original Draft, Supervision, Resources, Project Administration, Funding Acquisition, Conceptualization.

Declaration of competing interest

The authors declare that they have no known competing financial interests or personal relationships that could have appeared to influence the work reported in this paper.

Acknowledgments

This work was supported by the LIFE20 CCM/GR/001642 – LIFE CO_2toCH_4 of the European Union LIFE + program and the European Union's Horizon 2020 research and innovation program under grant agreement No 101084405 (CRONUS). We want to thank Prof. Irini Angelidaki and Dr. Antonio Grimalt-Alemany from the Department of Chemical and Biochemical Engineering at the Technical University of Denmark for providing the microbial inoculum used in the experiment and for their assistance in the study design.

Appendix A. Supplementary data

Supplementary data to this article can be found online at https://doi.org/10.1016/j.ese.2025.100637.

References

[1] A. Grimalt-Alemany, I.V. Skiadas, H.N. Gavala, Syngas biomethanation: State-of-the-art review and perspectives, Biofuel Bioprod. Biorefining 12 (2018) 139–158, https://doi.org/10.1002/bbb.1826.

[2] A. Galani, D. Sipkema, D.Z. Sousa, Hot prospects: harnessing thermophilic microbes for syngas fermentation, Trends Biotechnol. 0 (2025), https://doi.org/10.1016/j.tibtech.2025.04.017.

[3] Y. Jing, S. Campanaro, P. Kougias, L. Treu, I. Angelidaki, S. Zhang, G. Luo, Anaerobic granular sludge for simultaneous biomethanation of synthetic wastewater and CO with focus on the identification of CO-converting microorganisms, Water Res. 126 (2017) 19–28, https://doi.org/10.1016/j.watres.2017.09.018.

[4] H.N. Gavala, A. Grimalt-Alemany, K. Asimakopoulos, I.V. Skiadas, Gas biological conversions: the potential of syngas and carbon dioxide as production platforms, Waste Biomass Valoriz. 12 (2021) 5303–5328, https://doi.org/10.1007/s12649-020-01332-7.

[5] K. Asimakopoulos, M. Łężyk, A. Grimalt-Alemany, A. Melas, Z. Wen, H.N. Gavala, I.V. Skiadas, Temperature effects on syngas biomethanation performed in a trickle bed reactor, Chem. Eng. J. 393 (2020) 124739, https://doi.org/10.1016/j.cej.2020.124739.

[6] P. Postacchini, A. Grimalt-Alemany, P. Ghofrani-Isfahani, L. Treu, S. Campanaro, L. Menin, F. Patuzzi, M. Baratieri, I. Angelidaki, Carbon monoxide inhibition on acidogenic glucose fermentation and aceticlastic methanogenesis, Bioresour. Technol. 407 (2024) 131076, https://doi.org/10.1016/j.biortech.2024.131076.

[7] K. Asimakopoulos, A. Grimalt-Alemany, C. Lundholm-Høffner, H.N. Gavala, I.V. Skiadas, Carbon sequestration through syngas biomethanation coupled with H2 supply for a clean production of natural gas grade biomethane, Waste Biomass Valoriz. 12 (2021) 6005–6019, https://doi.org/10.1007/s12649-021-01393-2.

[8] E.M. Goonesekera, A. Grimalt-Alemany, E. Thanasoula, H.F. Yousif, S.L. Krarup, M.C. Valerin, I. Angelidaki, Biofilm mass transfer and thermodynamic constraints shape biofilm in trickle bed reactor syngas biomethanation, Chem. Eng. J. 500 (2024) 156629, https://doi.org/10.1016/j.cej.2024.156629.

[9] M. Diender, A.J.M. Stams, D.Z. Sousa, Pathways and bioenergetics of anaerobic carbon monoxide fermentation, Front. Microbiol. 6 (2015). https://www.frontiersin.org/articles/10.3389/fmicb.2015.01275. (Accessed 27 January 2023).

[10] E. Oelgeschläger, M. Rother, Carbon monoxide-dependent energy metabolism in anaerobic bacteria and archaea, Arch. Microbiol. 190 (2008) 257–269, https://doi.org/10.1007/s00203-008-0382-6.

[11] L. Daniels, G. Fuchs, R.K. Thauer, J.G. Zeikus, Carbon monoxide oxidation by methanogenic bacteria, J. Bacteriol. 132 (1977) 118–126, https://doi.org/10.1128/jb.132.1.118-126.1977.

[12] M. Diender, R. Pereira, H.J.C.T. Wessels, A.J.M. Stams, D.Z. Sousa, Proteomic analysis of the hydrogen and carbon monoxide metabolism of Methanothermobacter marburgensis, Front. Microbiol. 7 (2016). https://www.frontiersin.org/articles/10.3389/fmicb.2016.01049. (Accessed 8 December 2023).

[13] O. Meyer, L. Gremer, R. Ferner, M. Ferner, H. Dobbek, M. Gnida, W. Meyer-Klaucke, R. Huber, The role of Se, Mo and Fe in the structure and function of carbon monoxide dehydrogenase, Biol. Chem. 381 (2000) 865–876, https://doi.org/10.1515/BC.2000.108.

[14] J.-H. Jeoung, B.M. Martins, H. Dobbek, Carbon monoxide dehydrogenases, Methods Mol. Biol. Clifton NJ 1876 (2019) 37–54, https://doi.org/10.1007/978-1-4939-8864-8_3.

[15] M. Inoue, I. Nakamoto, K. Omae, T. Oguro, H. Ogata, T. Yoshida, Y. Sako, Structural and phylogenetic diversity of anaerobic carbon-monoxide dehydrogenases, Front. Microbiol. 9 (2019), https://doi.org/10.3389/fmicb.2018.03353.

[16] M.K. Nobu, T. Narihiro, C. Rinke, Y. Kamagata, S.G. Tringe, T. Woyke, W.-T. Liu, Microbial dark matter ecogenomics reveals complex synergistic networks in a methanogenic bioreactor, ISME J. 9 (2015) 1710–1722, https://doi.org/10.1038/ismej.2014.256.

[17] Y. Song, J.S. Lee, J. Shin, G.M. Lee, S. Jin, S. Kang, J.-K. Lee, D.R. Kim, E.Y. Lee, S.C. Kim, S. Cho, D. Kim, B.-K. Cho, Functional cooperation of the glycine synthase-reductase and wood–ljungdahl pathways for autotrophic growth of Clostridium drakei, Proc. Natl. Acad. Sci. 117 (2020) 7516–7523, https://doi.org/10.1073/pnas.1912289117.

[18] S. Jain, A. Katsyv, M. Basen, V. Müller, The monofunctional CO dehydrogenase CooS is essential for growth of Thermoanaerobacter kivui on carbon monoxide, Extrem. Life Extreme Cond. 26 (2021) 4, https://doi.org/10.1007/s00792-021-01251-y.

[19] S.W. Ragsdale, Enzymology of the wood-Ljungdahl pathway of acetogenesis, Ann. N. Y. Acad. Sci. 1125 (2008) 129–136, https://doi.org/10.1196/annals.1419.015.

[20] J. Seravalli, S.W. Ragsdale, Channeling of carbon monoxide during anaerobic carbon dioxide fixation, Biochemistry 39 (2000) 1274–1277, https://doi.org/10.1021/bi991812e.

[21] A.M. Bolger, M. Lohse, B. Usadel, Trimmomatic: a flexible trimmer for illumina sequence data, Bioinformatics 30 (2014) 2114–2120, https://doi.org/10.1093/bioinformatics/btu170.

[22] A. Prjibelski, D. Antipov, D. Meleshko, A. Lapidus, A. Korobeynikov, Using SPAdes De Novo Assembler, Curr. Protoc. Bioinform. 70 (2020) e102, https://doi.org/10.1002/cpbi.102.

[23] B. Langmead, S.L. Salzberg, Fast gapped-read alignment with bowtie 2, Nat. Methods 9 (2012) 357–359, https://doi.org/10.1038/nmeth.1923.

[24] P. Danecek, J.K. Bonfield, J. Liddle, J. Marshall, V. Ohan, M.O. Pollard, A. Whitwham, T. Keane, S.A. McCarthy, R.M. Davies, H. Li, Twelve years of SAMtools and BCFtools, GigaScience 10 (2021), https://doi.org/10.1093/gigascience/giab008 giab008.

[25] D.D. Kang, F. Li, E. Kirton, A. Thomas, R. Egan, H. An, Z. Wang, MetaBAT 2: an adaptive binning algorithm for robust and efficient genome reconstruction from metagenome assemblies, PeerJ 7 (2019) e7359, https://doi.org/10.7717/peerj.7359.

[26] J.N. Nissen, J. Johansen, R.L. Allesøe, C.K. Sønderby, J.J.A. Armenteros, C.H. Grønbech, L.J. Jensen, H.B. Nielsen, T.N. Petersen, O. Winther, S. Rasmussen, Improved metagenome binning and assembly using deep variational autoencoders, Nat. Biotechnol. 39 (2021) 555–560, https://doi.org/10.1038/s41587-020-00777-4.

[27] Y.-W. Wu, B.A. Simmons, S.W. Singer, MaxBin 2.0: an automated binning algorithm to recover genomes from multiple metagenomic datasets, Bioinformatics 32 (2016) 605–607, https://doi.org/10.1093/bioinformatics/btv638.

[28] S. Pan, X.-M. Zhao, L.P. Coelho, SemiBin2: self-supervised contrastive learning leads to better MAGs for short- and long-read sequencing, Bioinformatics 39 (2023) i21–i29, https://doi.org/10.1093/bioinformatics/btad209.

[29] A. Chklovski, D.H. Parks, B.J. Woodcroft, G.W. Tyson, CheckM2: a rapid, scalable and accurate tool for assessing microbial genome quality using machine learning, Nat. Methods 20 (2023) 1203–1212, https://doi.org/10.1038/s41592-023-01940-w.

[30] M.R. Olm, C.T. Brown, B. Brooks, J.F. Banfield, dRep: a tool for fast and accurate genomic comparisons that enables improved genome recovery from metagenomes through de-replication, ISME J. 11 (2017) 2864–2868, https://doi.org/10.1038/ismej.2017.126.

[31] R.M. Bowers, N.C. Kyrpides, R. Stepanauskas, M. Harmon-Smith, D. Doud, T.B.K. Reddy, F. Schulz, J. Jarett, A.R. Rivers, E.A. Eloe-Fadrosh, S.G. Tringe, N.N. Ivanova, A. Copeland, A. Clum, E.D. Becraft, R.R. Malmstrom, B. Birren, M. Podar, P. Bork, G.M. Weinstock, G.M. Garrity, J.A. Dodsworth, S. Yooseph, G. Sutton, F.O. Glöckner, J.A. Gilbert, W.C. Nelson, S.J. Hallam, S.P. Jungbluth, T.J.G. Ettema, S. Tighe, K.T. Konstantinidis, W.-T. Liu, B.J. Baker, T. Rattei, J.A. Eisen, B. Hedlund, K.D. McMahon, N. Fierer, R. Knight, R. Finn, G. Cochrane, I. Karsch-Mizrachi, G.W. Tyson, C. Rinke, A. Lapidus, F. Meyer, P. Yilmaz, D.H. Parks, A. Murat Eren, L. Schriml, J.F. Banfield, P. Hugenholtz, T. Woyke, Minimum information about a single amplified genome (MISAG) and a metagenome-assembled genome (MIMAG) of bacteria and archaea, Nat. Biotechnol. 35 (2017) 725–731, https://doi.org/10.1038/nbt.3893.

[32] P.-A. Chaumeil, A.J. Mussig, P. Hugenholtz, D.H. Parks, GTDB-Tk v2: memory friendly classification with the genome taxonomy database, Bioinformatics 38 (2022) 5315–5316, https://doi.org/10.1093/bioinformatics/btac672.

[33] S.T.N. Aroney, R.J.P. Newell, J.N. Nissen, A.P. Camargo, G.W. Tyson, B.J. Woodcroft, CoverM: read alignment statistics for metagenomics, Bioinformatics 41 (2025), https://doi.org/10.1093/bioinformatics/btaf147 btaf147.

[34] D. Hyatt, G.-L. Chen, P.F. LoCascio, M.L. Land, F.W. Larimer, L.J. Hauser, Prodigal: prokaryotic gene recognition and translation initiation site identification, BMC Bioinf. 11 (2010) 119, https://doi.org/10.1186/1471-2105-11-119.

[35] C.P. Cantalapiedra, A. Hernández-Plaza, I. Letunic, P. Bork, J. Huerta-Cepas, eggNOG-mapper v2: functional annotation, orthology assignments, and domain prediction at the metagenomic scale, Mol. Biol. Evol. 38 (2021) 5825–5829, https://doi.org/10.1093/molbev/msab293.

[36] M. Kanehisa, M. Furumichi, Y. Sato, M. Kawashima, M. Ishiguro-Watanabe, KEGG for taxonomy-based analysis of pathways and genomes, Nucleic Acids Res. 51 (2023) D587–D592, https://doi.org/10.1093/nar/gkac963.

[37] A.P. Camargo, S. Roux, F. Schulz, M. Babinski, Y. Xu, B. Hu, P.S.G. Chain, S. Nayfach, N.C. Kyrpides, Identification of Mobile genetic elements with geNomad, Nat. Biotechnol. (2023) 1–10, https://doi.org/10.1038/s41587-023-01953-y.

[38] S. Nayfach, A.P. Camargo, F. Schulz, E. Eloe-Fadrosh, S. Roux, N.C. Kyrpides, CheckV assesses the quality and completeness of metagenome-assembled viral genomes, Nat. Biotechnol. 39 (2021) 578–585, https://doi.org/10.1038/s41587-020-00774-7.

[39] D. Li, C.-M. Liu, R. Luo, K. Sadakane, T.-W. Lam, MEGAHIT: an ultra-fast single-node solution for large and complex metagenomics assembly via succinct de Bruijn graph, Bioinformatics 31 (2015) 1674–1676, https://doi.org/10.1093/bioinformatics/btv033.

[40] S. Roux, E.M. Adriaenssens, B.E. Dutilh, E.V. Koonin, A.M. Kropinski, M. Krupovic, J.H. Kuhn, R. Lavigne, J.R. Brister, A. Varsani, C. Amid, R.K. Aziz, S.R. Bordenstein, P. Bork, M. Breitbart, G.R. Cochrane, R.A. Daly, C. Desnues, M.B. Duhaime, J.B. Emerson, F. Enault, J.A. Fuhrman, P. Hingamp, P. Hugenholtz, B.L. Hurwitz, N.N. Ivanova, J.M. Labonté, K.-B. Lee, R.R. Malmstrom, M. Martinez-Garcia, I.K. Mizrachi, H. Ogata, D. Páez-Espino, M.-A. Petit, C. Putonti, T. Rattei, A. Reyes, F. Rodriguez-Valera, K. Rosario, L. Schriml, F. Schulz, G.F. Steward, M.B. Sullivan, S. Sunagawa, C.A. Suttle, B. Temperton, S.G. Tringe, R.V. Thurber, N.S. Webster, K.L. Whiteson, S.W. Wilhelm, K.E. Wommack, T. Woyke, K.C. Wrighton, P. Yilmaz, T. Yoshida, M.J. Young, N. Yutin, L.Z. Allen, N.C. Kyrpides, E.A. Eloe-Fadrosh, Minimum information about an uncultivated virus genome (MIUViG), Nat. Biotechnol. 37 (2019) 29–37, https://doi.org/10.1038/nbt.4306.

[41] A. Zielezinski, A. Gudyś, J. Barylski, K. Siminski, P. Rozwalak, B.E. Dutilh, S. Deorowicz, Ultrafast and accurate sequence alignment and clustering of viral genomes, Nat. Methods 22 (2025) 1191–1194, https://doi.org/10.1038/s41592-025-02701-7.
[42] A.J. Hockenberry, C.O. Wilke, BACPHLIP: predicting bacteriophage lifestyle from conserved protein domains, PeerJ 9 (2021) e11396, https://doi.org/10.7717/peerj.11396.
[43] S. Roux, A.P. Camargo, F.H. Coutinho, S.M. Dabdoub, B.E. Dutilh, S. Nayfach, A. Tritt, iPHoP: an integrated machine learning framework to maximize host prediction for metagenome-derived viruses of archaea and bacteria, PLoS Biol. 21 (2023) e3002083, https://doi.org/10.1371/journal.pbio.3002083.
[44] G.H. Putri, S. Anders, P.T. Pyl, J.E. Pimanda, F. Zanini, Analysing high-throughput sequencing data in python with HTSeq 2.0, Bioinformatics 38 (2022) 2943–2945, https://doi.org/10.1093/bioinformatics/btac166.
[45] M.I. Love, W. Huber, S. Anders, Moderated estimation of fold change and dispersion for RNA-Seq data with DESeq2, Genome Biol. 15 (2014) 550, https://doi.org/10.1186/s13059-014-0550-8.
[46] J. Figueras, H. Benbelkacem, C. Dumas, P. Buffiere, Syngas biomethanation: study of process performances at high syngas flow rate in pressurized stirred column, Bioresour. Technol. 376 (2023) 128936, https://doi.org/10.1016/j.biortech.2023.128936.
[47] D. Susanti, J.H. Wong, W.H. Vensel, U. Loganathan, R. DeSantis, R.A. Schmitz, M. Balsera, B.B. Buchanan, B. Mukhopadhyay, Thioredoxin targets fundamental processes in a methane-producing archaeon, *Methanocaldococcus jannaschii*, Proc. Natl. Acad. Sci. 111 (2014) 2608–2613, https://doi.org/10.1073/pnas.1324240111.
[48] A. Rossi, M.S. Morlino, M. Gaspari, A. Basile, P. Kougias, L. Treu, S. Campanaro, Analysis of the anaerobic digestion metagenome under environmental stresses stimulating prophage induction, Microbiome 10 (2022) 125, https://doi.org/10.1186/s40168-022-01316-w.
[49] H. Georjon, A. Bernheim, The highly diverse antiphage defence systems of bacteria, Nat. Rev. Microbiol. 21 (2023) 686–700, https://doi.org/10.1038/s41579-023-00934-x.
[50] B. Kakuk, R. Wirth, G. Maróti, M. Szuhaj, G. Rakhely, K. Laczi, K.L. Kovács, Z. Bagi, Early response of methanogenic archaea to H2 as evaluated by metagenomics and metatranscriptomics, Microb. Cell Fact. 20 (2021) 127, https://doi.org/10.1186/s12934-021-01618-y.